Manuscript submitted to: Volume 2, Issue 2, 116-132.

AIMS Energy DOI: 10.3934/energy.2014.2.116

Received date 7 February 2014, Accepted date 24 March 2014, Published date 5 April 2014

Research Article

Spray-combustion process characterization in a common rail diesel engine fuelled with butanol-diesel blends by conventional methods and optical diagnostics

Simona Silvia Merola *, Luca Marchitto, Cinzia Tornatore and Gerardo Valentino

Istituto Motori –CNR, Via G. Marconi 4 - 80125 Napoli, Italy

* **Correspondence:** Email: s.merola@im.cnr.it; Tel: +39-081-717-7224; Fax: +39-081-239-6097.

Abstract: The target of a sustainable mobility has led to investigate advanced combustion modes and fuels technologies. On the other side, the increasing global energy demand and the decreasing fossil-energy resources are enhancing the interest in the use of renewable alternative fuels for compression ignition engines with the target of near-zero emission levels. Although performance and emissions of alternative-fuel within light-duty diesel engines have been extensively investigated, results of fuel chemical composition impact on combustion by integrated optical methodologies are lacking. In order to meet this challenge, one of the main objectives of the research efforts is to characterize the combustion and species evolution. In this investigation, conventional tests and optical diagnostics were employed to enhance the comprehension of the combustion process and chemical markers in a common rail compression ignition engine powered by butanol-diesel blends. The investigation was focused on the effect of the injection strategy and blend composition on in-cylinder spray combustion and soot formation, through UV-visible digital imaging and natural emission spectroscopy. Experiments were performed in an optically accessible single cylinder high swirl compression ignition engine, equipped with a common rail multi-jets injection system. UV-visible emission spectroscopy was used to follow the evolution of the combustion process chemical markers. Spectral features of OH were identified and followed during the spray combustion process examining different pilot-main dwell timings. Soot spectral evidence in the visible wavelength range was correlated to soot engine out emissions. In this work, conventional and optical data related to diesel fuel blended with 40 % of n-butanol will be presented.

Keywords: Combustion; Common rail diesel engine; Butanol fuel; Diesel fuel; Optical diagnostics; Chemiluminescence.

1. Introduction

The necessity to change from an economy that is largely based on non-renewable fossil fuels as raw materials to one that is based on renewable sources is a worldwide challenge. Two fundamental drivers lead this challenge: the first is a growing world demand for crude oil, as a result of the rapidly growing economies of China and other BRIC countries coupled with political instability in many areas of the world in which the major crude oil exporters are situated; the second is the need to reduce net emissions and environmental impact of carbon dioxide and other greenhouse gases (GHG) associated with the consumption of fossil fuels and thereby the environmental footprint of fuels and chemicals production. In this scenario, biodiesel from biomass and other non-food feed-stocks can be considered the primary alternative to diesel fuel due to its properties close to diesel fuel and its miscibility with diesel in any percentage [1,2]. Recently, it is growing the interest in the use of alcohols as a viable alternative either single or blended with conventional based fuels. In particular, the first four aliphatic alcohols (methanol, ethanol, propanol and butanol) are of interest as fuels because they can be synthesized biologically [3,4]. Further, they have physical and chemical properties such as less carbon and sulphur content, and more oxygen than traditional fossil-based fuels [5], this allows them to be applied in current engines. As one of the primary alcohol fuels, butanol has more advantages than methanol and ethanol as an alternative fuel for internal combustion engines. In fact, butanol has a lower auto-ignition temperature than methanol and ethanol, so it can be ignited easier when burned in diesel engines. Besides, butanol has lower volatility and higher energy density than ethanol and methanol. In addition, butanol has lower water adsorption and corrosive properties. Butanol can be produced by fermentation of biomass, such as algae, corn, and other plant materials containing cellulose that could not be used for food and would otherwise go to waste [6,7]. Recent use of genetically enhanced bacteria has increased the fermentation process productivity, even if more work is necessary to make butanol production economically viable [8,9]. The butanol cost is still an important disadvantage, but the benefits of the blending with diesel are likewise important. If compared with other alcohols, as methanol and ethanol, butanol has better solubility with diesel thus avoiding the use of additives, viscosity similar to diesel fuel and has the ability to be used in conventional internal combustion engines without the need for modification [10-12]. This allows the electronic control high pressure common rail fuel injection system to realize a flexible and precise control of fuel injection [13-15].

It is known that large reduction of emissions can be achieved by applying multiple injection strategies [16]. Soot emission can be reduced by raising the injection pressure to accelerate fuel evaporation through production of smaller fuel droplets, enhance fuel-air mixing and create faster combustion rates. Moreover, by injecting a small amount of fuel as pilot before the main injection, it is possible to reduce combustion noise by limiting the amount of premixed combustion. The strategy leads to a decrease in-cylinder pressure rise rate, and thus the reduction of the combustion noise. The effect of pilot injection on the exhaust emissions is linked to the injection timing. A long dwell time between pilot and main injection reduces particulate emissions with higher efficiency at high load. On the other hand, at medium-low load, a small dwell time allowed to reduce premixed burn fraction and NOx. Regarding the use of butanol as fuel for compression ignition engines, previous investigations [11,17] showed that butanol, blended with diesel until 40 % in volume (BU40), increased combustion pressure and accelerated burning rate, while having little impact on maximum power and torque output. Moreover, butanol-diesel blends slightly increased BSFC (Brake Specific

Fuel Consumption) but attained a higher thermal efficiency than the neat diesel fuel. The effects of butanol addition to diesel fuel on emissions were strongly influenced by EGR and loads. In general, HC emissions of blends were higher than the neat diesel, especially under low-loads. In these conditions, as expected, CO emissions increased while NOx emissions decreased as butanol blending ratio increased. Under high-load conditions, on the contrary, CO emissions decreased but NOx emissions increased. Moreover, butanol-diesel blends significantly reduce soot emissions in all conditions, and the reduction is higher at increasing blending ratio. In conclusion, butanol is a promising biofuel, which can be used conveniently and advantageously up to high blending ratio with diesel fuel (BU40), both from the viewpoints of thermal efficiency and soot emission.

Even if scientific literature reports numerous experimental investigations to evaluate the effects of butanol-diesel blends on performance, exhaust emissions and combustion behaviour for different engine operating conditions, more data are required to better understand the basis physical and chemical phenomena related to the direct injection and the spray combustion process. For example, an improved knowledge of butanol effects on multi-injection spray combustion processes is useful to reach the fuel flexibility and NOx-PM trade off optimization. Moreover, these experiments provide fundamental support for kinetic chemical modelling and 1D—3D simulation codes.

For all these reasons, UV-visible flame emission spectroscopy was applied in the combustion chamber of single cylinder high swirl compression ignition engine equipped with a common rail multi-jets injection system. This optical methodology is a powerful diagnostic because natural emissions from diesel flame consist of both chemiluminescence and soot luminosity [18]. Chemiluminescence is produced by the excitation of the intermediate combustion radicals due to exothermic chemical reactions occurring during the auto-ignition and combustion process [19]; soot luminosity is caused by the emissions from hot soot particles and it is characterized by a continuous broadband spectrum similar to the Planck black body emission curve [20,21].

All the combustion tests were performed fuelling the optical accessible engine with a commercial diesel (BU00) and a blend of 60 % diesel with 40 % n-butanol (BU40). The combustion process was studied from injection until the late combustion phase, fixing the injection pressure at 70MPa and changing the pilot injection timing. Optical results were correlated with the engine parameters and with exhaust emissions.

2. Experimental Apparatus

The engine used in the work is an external high swirl optically accessible combustion bowl connected to a single cylinder 2-stroke high pressure common rail compression ignition engine. The main engine specifications are reported in Table 1. The external combustion bowl (50 mm in diameter and 30 mm in depth) is suitable to stabilize, at the end of compression stroke, swirl conditions to reproduce the fluid dynamic environment similar to those within a real direct injection diesel engine. The implication of “cylindrical bowl” is related to the peculiar design of the prototype engine that has a large displacement as an air compressor. The main cylinder, connected to the external “swirled bowl” through a tangential duct, allows supply of compressed air to flow to the bowl as the piston approaches TDC. The air flow, coming from the cylinder, is forced within the combustion chamber by means of the tangential duct. In this way, a counter clockwise swirl flow, with the rotation axis about coincident to the symmetry axis of the chamber, is generated. The injector was mounted within this swirled chamber with its axis coincident to the chamber axis; in this

way the injected fuel is mixed through a typical interaction with the swirling air flow. The combustion process starts and mainly goes on in the chamber. After a few crank angles the piston moves downward, the flow reverses its motion and the hot gases flow through the tangential duct to the cylinder and finally to the exhaust ports. The combustion chamber provides both a circular optical access (50 mm diameter), on one side of it, used to collect images and a rectangular one (size of 10 x 50 mm) at 90°, outlined on the cylindrical surface of the chamber, used for the laser illumination input. The injection equipment includes a common rail injection system with a solenoid controlled injector located on the opposite side of the circular optical access. The nozzle is a micro-sac 7 hole, 0.141 mm diameter, 148° spray angle nozzle. An external roots blower provided an absolute air pressure at the inlet of 0.21 MPa with a peak pressure within the combustion chamber of 4.9 MPa under motored conditions. The pressure in the swirl combustion chamber was measured by a quartz pressure transducer with the assumption of no pressure difference between the swirl and the main cylinder chamber.

The injection duration was calibrated for delivering the same mass of fuel by changing the butanol concentration: 30 mg/stroke. Even if the n-butanol density (810 g/dm^3) is similar to the Diesel one (832 g/dm^3), the other fluid-dynamic properties (e.g. viscosity) could affect the fuel mass injection rate. The injection time was found to be the same for the main injection (990 μs); the pilot injection was set at 420 μs for Butanol blends and 400 μs for pure Diesel. Measurements were performed using the gravimetric method for 1200 consecutive injections, with an accuracy of 0.01 %.

Table 1. Specifications of the engine

2-stroke single cylinder engine	
Cylindrical Bowl (mmxmm)	50x30
Bore (mm)	150
Stroke (mm)	170
Connecting Rod (mm)	360
Compression ratio	10.1:1
Air supply	Roots Blower
Outlet/Inlet Blower Ratio	2.1
Bosch Injector nozzle	7/0.141/148°

During the spectroscopic investigations, the radiative emissions from the combustion chamber were focused by a 78 mm focal length, f/3.8 UV Nikon objective onto the micrometer controlled entrance slit of a spectrometer (Acton SP2150) with 150 mm focal length and 600 groove/mm grating. The central wavelength of the grating was fixed at 300 and 400 nm. From the grating the radiations were detected by an intensified CCD camera (PI-MAX3-Princeton Instruments). The camera has an array size of 1024 x 1024 pixels with a pixel size of 13 x 13 μm and 16-bit dynamic range digitization at 100 kHz. The exposure time was fixed at 42 μs and the dwell time between two consecutive acquisitions was set at 62 μs.

Spectroscopic investigations were carried out in the central region of the combustion chamber, divided in 8 locations. Figure 1 shows the sketches of the experimental apparatus for the optical

investigations. To enhance signal to noise ratio the 64 spectra of each location were averaged. The flame emission spectra were corrected for the optical setup efficiency using a deuterium lamp with a highly uniform full spectrum. The wavelength calibration was performed using a mercury lamp. The time evolution of combustion products was evaluated from spectroscopic investigations using a post-processing procedure. For each chemical species, with well-resolvable narrow emission bands, the height of the band was evaluated after the subtraction of emission background and other species contribution. Software, developed in Labview environment, allowed simultaneous evaluation of the emissions of the selected compounds and species for each spectrum and time. OH and soot emissions were calculated as average on all the spectra. The optical set-up was used also for UV-visible digital imaging of the spray combustion process to support the spectroscopic investigations. In particular, the central wavelength of the spectrometer was fixed at 0 (in this way the device worked as a mirror) and the input slit was opened (3 mm width). The exposure time and the acquisition timing were maintained unchanged.

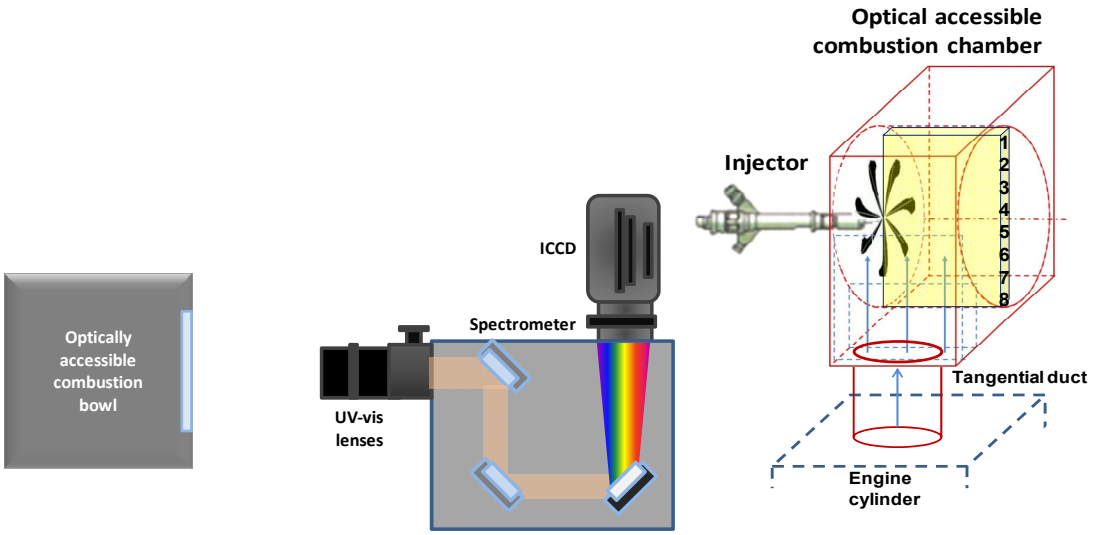

Figure 1. Sketches of the experimental apparatus for the optical investigations. The locations for the spectroscopic investigations are number labelled.

Combustion tests were carried out using three blends. The baseline fuel was the European low sulphur (10 ppm) commercial diesel with a cetane number of 52 (BU00). Moreover, blends of butanol (20 %)—diesel (80 %) (by vol.) (BU20) and butanol (40 %)—diesel (60 %) (BU40) were tested. The main properties of the fuels are reported in Table 2.

All the experimental data were collected using the AVL INDICOM driven by an optical encoder with 0.1 crank angle degree resolution. The pressure in the swirl chamber was measured by a quartz pressure transducer AVL QC34C. Results of the in-cylinder pressure were computed over 300 consecutive engine cycles. Exhaust gaseous emissions were acquired by AVL DiGas 4000 analyser for NOx, the Smoke Meter AVL 415S was used for FSN measurements. The accuracy of the acquired quantities was 10ppm for NOx and 0.1 % for smoke.

Table 2. Fuel properties.

	BU00	BU20	BU40
Density @15 °C (kg/m^3) ASTM D4052	840	830	826
Cetane number ISO4264	52	44	36
Net heat value (MJ/kg)	42.5	41	36.9
Carbon content (%) ASTM D5291	87	80.2	75.19
Hydrogen content (%) ASTM D5291	12.6	15.4	16.8
Oxygen content (%) ASTM D5291	–	4.32	8.64
IBP (°C) ASTM D86	160	139	117
Distillation 50% vol. (°C) ASTM D86	280	250	226
Distillation 90% vol. (°C) ASTM D86	338	328	325

3. Results and Discussion

3.1. Engine parameters and exhaust measurements

Engine tests were carried out at 500 rpm; 30 mg ± 1% of fuel was injected at the pressure of 70 MPa setting a double injection (pilot and main). In the present paper, the SOI indicates the start of the energizing current to the solenoid injector. Because of the hydraulic and electronic delay a shift between the timing of the energizing current to the solenoid (SOI) and the fuel delivery from the injector nozzles (FSOI) is produced; this delay was estimated in 340 μs from the measurement of the instantaneous fuel flow rate.

Preliminary investigations were performed to evaluate the effect of the pilot injection timing at fixed main injection timing for reference diesel fuel. The start of main injection was set at 11 and 3 CAD BTDC while the start of pilot injection was swept to obtain a pilot-main dwell time of 8, 6 and 4 CAD for both main injections. Figures 2-3 show the exhaust measurements (smoke and NO_x). In Figure 4 the engine combustion work versus pilot-main injection dwell crank angle is plotted. The engine combustion work (ECW) was evaluated as the percentage variation of the area under the pressure signal in the fired (Af) and motored condition (Am) [22].

$$\boldsymbol{ECW = \frac{A_f - A_m}{A_m} * 100}$$

This parameter may be correlated to the combustion efficiency of the selected fuel injection strategy. Experiments demonstrated that advanced start of main injection induced a strong decrease (>80 %) in the exhaust smoke for all pilot injection timings. On the other hand, the expected increase in the NOx emission was about 50 % and it was matched by an increase in net engine working cycle higher than 40 %. All the injection strategies attained the autoignition of pilot and main before the end of fuel delivery from the nozzle, inducing a mixing controlled combustion regime (MCC). To substantiate this statement, a selection of spray combustion images, detected fixing the SOI of pilot injection at -17 CAD ATDC, is reported in Figure 5. As a consequence of these results, the investigation was focused on the effect of butanol-diesel blends fixing the main injection at 11 CAD BTDC.

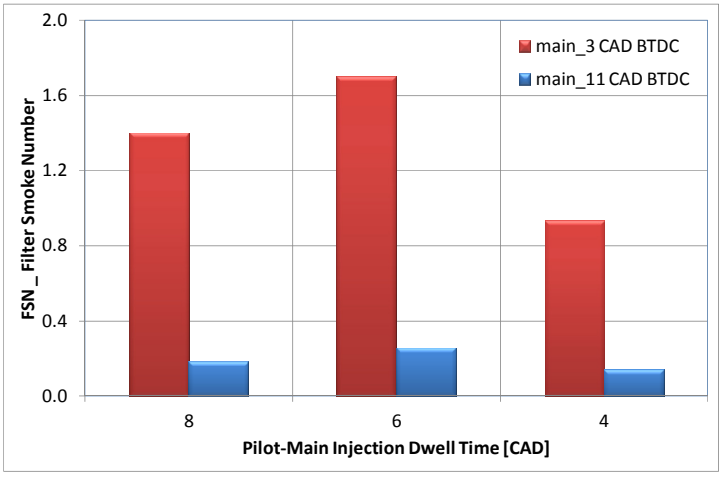

Figure 2. Engine emissions of smoke (FSN) vs Pilot-Main dwell time for BU00.

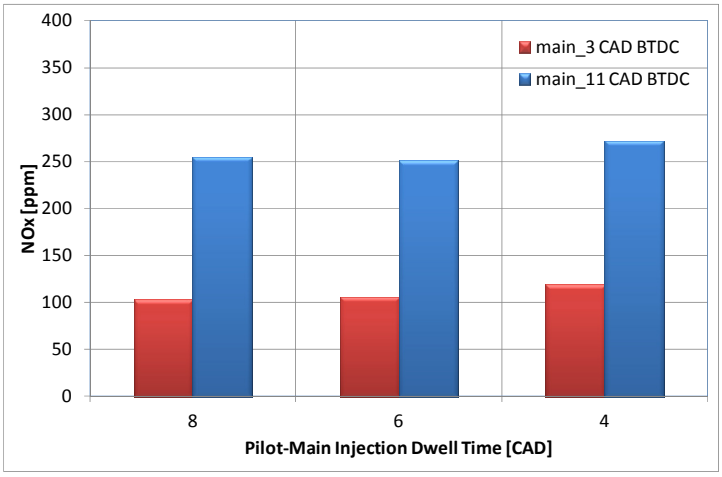

Figure 3. Engine emissions of NOx vs Pilot-Main dwell time for BU00.

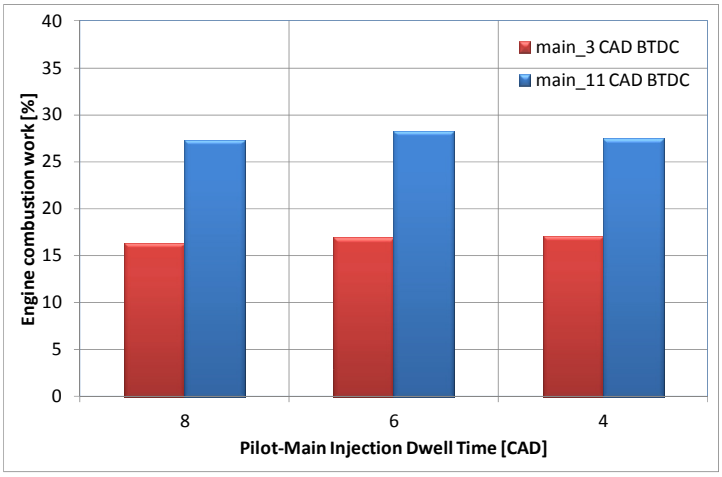

Figure 4. Percentage engine combustion work vs Pilot-Main dwell time for BU00.

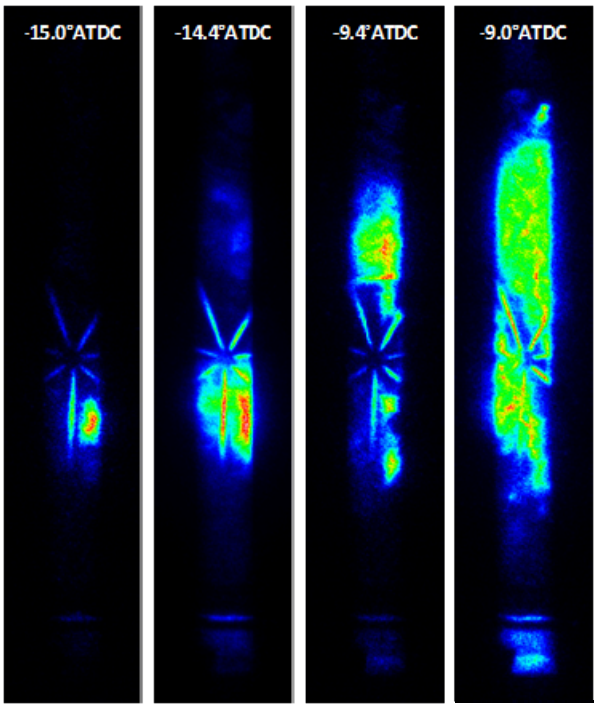

Figure 5. Images detected during the BU00 spray combustion for the double strategy, setting the pilot injection 17 CAD BTDC and the main injection at 11 CAD BTDC.

Following the previous studying approach, Figures 6–8 show smoke and NO_x exhaust emission, and the net engine working cycle percentage for diesel and butanol blends fixing the main injection at 11 CAD BTDC at different pilot-main dwell time. Even if the diesel smoke number resulted already low for diesel, butanol induced a further decrease in soot exhaust emission as butanol blending ratio increased. The effect was expected due to the lower carbon content, the better mixing related to the higher volatility of butanol blends and the presence of oxygen within the butanol molecule. The highest reduction in smoke was obtained setting the dwell time at 6 CAD. The increase in butanol volume fraction produced an appreciable rise in NO_x emissions only for BU40 with a slight effect given by the dwell-time. Regarding the combustion efficiency, the net engine working area increased at higher butanol volume fraction. Again, the increase was influenced by the fuel properties while a minor effect was due to the pilot injection timing.

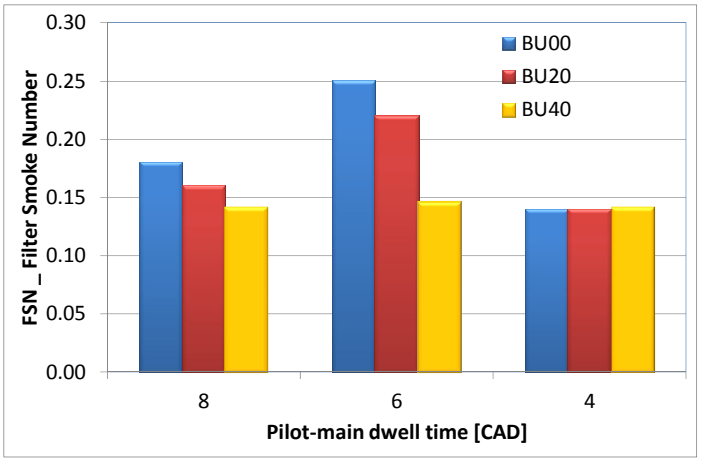

Figure 6. Engine exhaust emissions of smoke (FSN) vs Pilot-Main dwell time for selected fuels at fixed SOI of main injection (11 CAD BTDC).

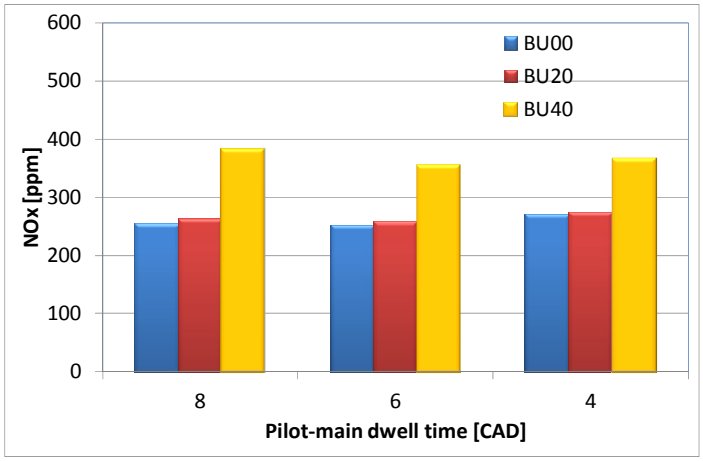

Figure 7. Engine exhaust emissions of NOx vs Pilot-Main dwell time for selected fuels at fixed SOI of main injection (11 CAD BTDC).

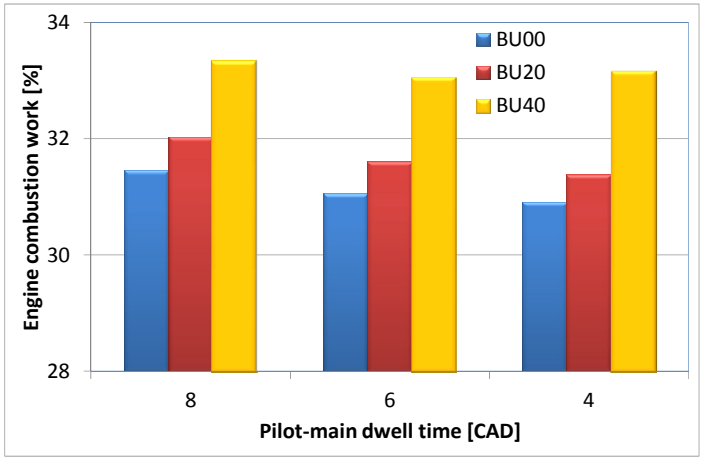

Figure 8. Percentage engine combustion work vs Pilot-Main dwell time for selected fuels at fixed SOI of main injection (11 CAD BTDC).

3.2. Optical results

To better understand the fuel injection strategy outcome on the combustion process, natural emission spectroscopy measurements were performed. For brevity, in this work the spectra detected setting the pilot injection at SOI = 15 CAD BTDC are reported. Figure 9 shows the first spectroscopic evidence of combustion process due to the pilot auto-ignition for both fuels. It can be noted that BU40 pilot combustion started around 0.2 CAD after diesel pilot combustion.

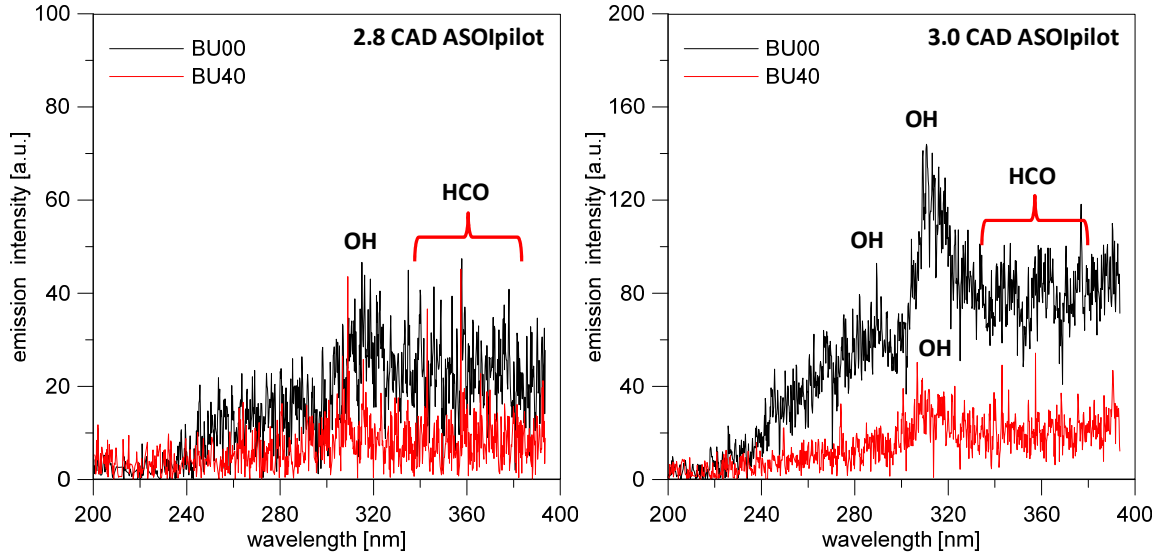

Figure 9. Flame emission spectra detected at the autoignition of pilot injection for BU00 and BU40 (SOIpilot 15 CAD BTDC; SOImain 11 CAD BTDC).

For both fuels, the pilot auto-ignition was characterised by the OH emissions due to the A2Σ+→X2Π transitions. Table 3 lists the heads of A-X system with an estimation of their intensities [23]. The most intense bands are centred around 280 nm and 309 nm. Excited OH radical is representative of the primary combustion zone and it is produced by the radiative chemical reaction CH + O2 → CO + OH [24]. Hydroxyl radicals exist both in the flame front and hot post-combustion gases. Moreover, the relative balance between the two bands (280 and 309 nm) is frequently used for flame temperature investigations [25]. It should be noted an auto-ignition delay of 0.2 CAD for butanol blend with respect to diesel due to different heating values (Table 2).

In the Diesel spectra of Figure 9, OH is superimposed on a broadband chemiluminescence. This was determined by the Vaidya's band system of HCO with highest heads from 290 nm to 360 nm and by the tail of Emeleus' bands due to excited formaldehyde molecule CH_2O^* (350 – 460 nm) [26]. The identification of the Vaidya hydrocarbon flame band emitters and their formation mechanisms are complex and have been the subject of much reference speculations [27,28]. Among this, it should be noted the reaction of formaldehyde with a free atom or radicals (O, H, OH, or alkyl radical) that induced HCO* formation [Error! Bookmark not defined.].

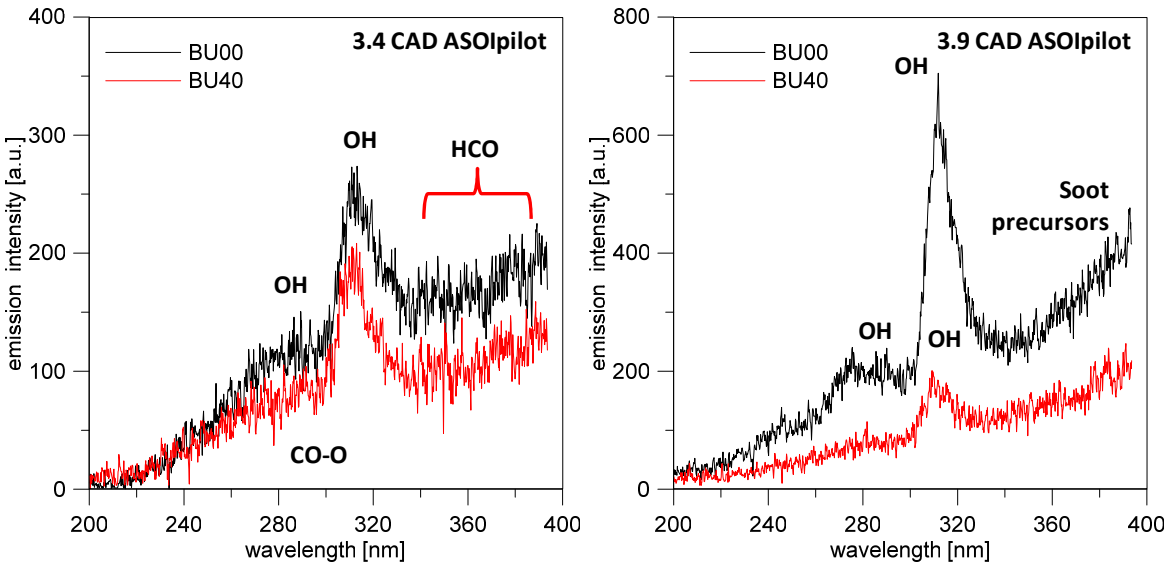

Figure 10. Flame emission spectra detected at 3.4 CAD (left) and 3.9 CAD (right) after pilot injection for BU00 and BU40 (SOIpilot 15 CAD BTDC; SOImain 11 CAD BTDC).

Table 3. Heads of the bands in A 2Σ+ → X2Π transitions. The related intensities are in the brackets [23].

(ν',ν")	0	1	2	3	4
0	306.4 (12)	342.8 (7)			
1	281.1 (9)	312.2 (9)	318.5 (6)		
2	260.9 (4)	287.5 (9)	308.5 (10)		
3	244.4 (1)	267.7 (5)	294.5 (7)	325.4 (4)	
4		251.7 (2)	275.3 (4)	302.2 (5)	333.1 (4)

After the auto-ignition timing the spectra evolved with similar features; moreover, in about 0.5 CAD, butanol-blend reduced the gap of intensity. As shown in Figure 10 (left), for both fuels at 3.4 CAD ASOI pilot, OH and HCO emissions are added to a weak blue continuum. This emission is due to the chemiluminescence accompanying the recombination of CO and O [28]: $CO(X^1\Sigma+)+O(^3P)\rightarrow CO_2(X^1\Sigma+g)+h\nu$. It occurred between 250 and 800 nm with a maximum intensity around 400 nm. The broad emission is also featured by the CO and CO_2^+ band systems present on the whole range of wavelengths. After around 0.5 CAD, the speed of flame propagation doubled in the emission intensity (Figure 10 right); in particular, the increase in the burned mass fraction and local temperature gave rise to an increase in OH emissions and consequently in the radical concentration. It should be noted that CO_2* evidence resulted unchanged, due to the fast transition to the ground state that induced the increase in neutral molecules [28]. For diesel, at 3.9 CAD ASOI pilot, the spectral evidence of a blue flame emission due to carbonaceous structures and soot nano-precursors was observed [29,30]. After the ignition of main injection (but during the fuel delivery period) the flame spreads across the combustion chamber. Spectra were characterised by a strong soot emission featured by a broadband signal that increased with the wavelength like a

blackbody curve, as shown in Figure 11 left [20,30]. Soot emission and thus soot concentration was lower for BU40 than diesel. The relative intensity between the two fuels remained unchanged during the combustion process, as shown in the right plot of Figure 11. Moreover, BU00 showed comparable emission intensity of the two OH band systems at 310 nm and 280 nm due to (0, 0) and (1, 0) of the A-X system, while for BU40 only the emission due to diagonal transition was well resolved. This optical evidence persisted until the late combustion phase in which the oxidation mechanism reduced the soot and highlighted the OH emission. The effect is well observed in Figure 12, which shows the spectra detected at 12.7 CAD ATDC (27.7 ASOI pilot) for both fuels. The relative emission intensity of OH at 280 and 310 nm is correlated to the adiabatic flame temperature. As expected, it is lower for BU40. Even if this contributed to reduce the NO formation rate, the significantly higher oxygen availability of BU40 induced local conditions nearer to stoichiometric compared to the neat diesel fuel operation. This works towards higher NOx liability in agreement with exhaust data.

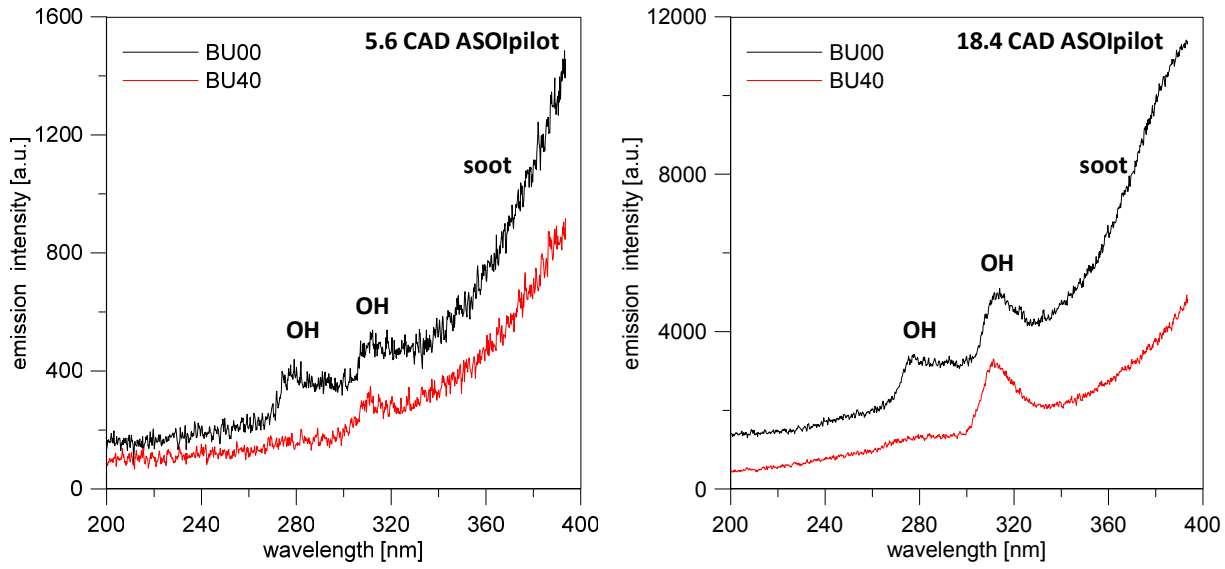

Figure 11. Flame emission spectra detected 5.6 CAD (left) and 18.4 CAD (right) after pilot injection for BU00 and BU40 (SOIpilot 15 CAD BTDC; SOImain 11 CAD BTDC).

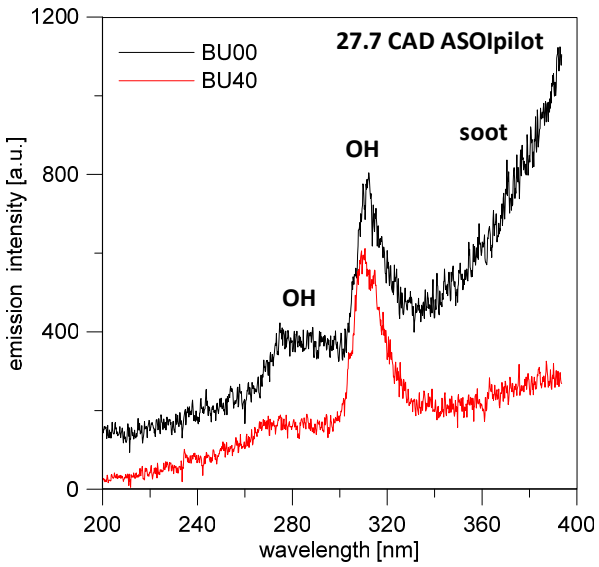

Figure 12. Flame emission spectra detected 27.7 CAD after pilot injection for BU00 and BU40 (SOIpilot 15 CAD BTDC; SOImain 11 CAD BTDC).

In order to better understand the effect of fuel and injection strategy on the combustion process, the soot and OH behaviours were evaluated. In particular, OH (0, 0) emission was measured as height of the 310 nm band system after the subtraction of the emission background, evaluated as the mean value between the emissions measured at 300 nm and 320 nm. Soot emission was evaluated as mean intensity at 500 nm using data obtained fixing 400 nm as central wavelength. OH and soot evolutions for SOIpilot 15 CAD BTDC are plotted in Figure 13.

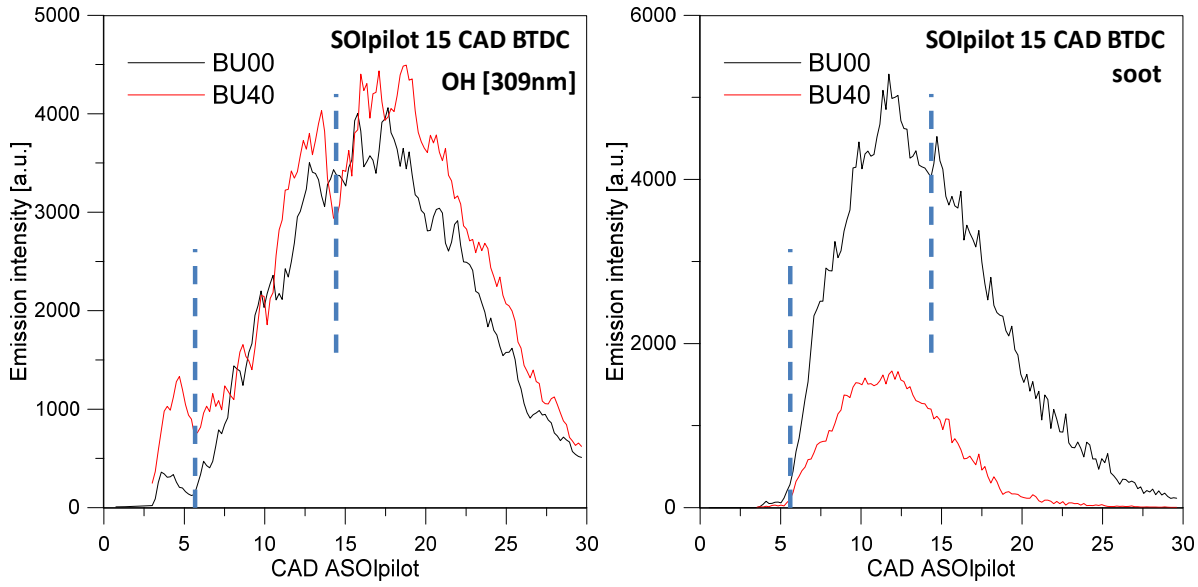

Figure 13. Time evolution of the OH (left) and soot (right) emission for both fuels (SOIpilot 15 CAD BTDC; SOImain 11 CAD BTDC).

OH radical in Figure 13 (left) progressed following three phases: the first one was due to the pilot ignition and it can be observed for around 5 CAD (first dashed line) after the pilot injection; at this time the main injection started and OH was generated by the ignition of the fuel delivered by the main injection involved with the mixed controlled combustion. In this phase, as shown in the right plot of Figure 13, the soot concentration began to rise up to the end of the main injection. Afterwards, starting from 14 CAD (second dashed line) after the pilot injection, the oxygenated species, including OH radicals, acted to quickly reduce the soot concentration. It is also evident that there is significant difference in soot emission intensity given by the BU40 with respect to the diesel fuel.

Similar trends were detected for the other fuel injection strategies with different pilot injection timings. The increasing in the pilot-main dwell time decreased the OH concentration in the first phase for both fuels, and reduced the difference between the two fuels. This effect was related to the lower pressure and temperature within the combustion chamber, at the pilot injection timing, that influenced the auto-ignition because of the small amount of injected fuel. The heat released by the pilot obviously influenced the main injection combustion; in particular, increasing the dwell time between pilot and main, the auto-ignition of the fuel delivered by the main injection was delayed and the OH formation rate decreased. As a consequence, the soot formation was increased by a simultaneous OH oxidation action. Finally, the OH evolution during the main injection combustion was opposite to that observed for pilot injection combustion. This was due to the lower temperature gradient and lower oxygen concentration in the combustion chamber during the main injection combustion. These effects were more evident for BU40 due to higher oxygen concentration in the fuel. As consequence of these phenomena, soot concentration was lower for BU40, as also confirmed by the exhaust measurements, and the discrepancy between the two fuels decreased with the pilot-main dwell time.

In conclusion, it may be highlighted that the effect of butanol was well marked during the soot formation phase. This occurred because soot formation, caused by high temperature fuel decomposition, mainly takes place in the fuel-rich zone at high temperatures and pressures, specifically within the core region of each fuel spray. If the fuel is partially oxygenated, as in the case of butanol blends, it has the ability to reduce locally fuel-rich regions and limit soot formation, reducing smoke opacity. Moreover, butanol blends are characterized by a lower stoichiometric air-fuel ratio (less air is needed to achieve stoichiometry and consequently complete combustion), which reduces the existence of fuel-rich regions in the non-uniform fuel-air mixture. Finally, the absence of aromatic compounds in butanol blends reduces the concentration of soot precursors.

4. Summary

In this paper, the effects of the injection strategy on the combustion process, comparing the baseline diesel to a blend of diesel and n-butanol (40 % by vol.), was experimentally investigated through UV-visible flame emission spectroscopy. Tests were performed within a single cylinder, high swirl compression ignition engine, optically accessible, equipped with a common rail multi-jets injection system. The investigation was carried out setting the start of the main injection at 11 CAD BTDC, for different dwell timings between the pilot and the main injections. The strategy allowed operating under a dominant mixed controlled combustion for both fuels. Spectroscopic investigation allowed following temporal and spatial evolution of the combustion process chemical markers, with particular interest for OH radicals and soot.

At fixed fuel injection strategies, BU40 showed higher combustion efficiency combined with lower soot emission and higher OH concentration (310 nm). This result was due to the oxygen content within the butanol blend and its higher volatility that enhanced mixing and promoted a better homogeneity of the vapour within the combustion chamber.

Regarding the effect of fuel injection strategy, the reduction of pilot-main dwell time, increased the OH (310nm) emission of the burnt fuel delivered during the pilot injection, both for the baseline diesel and the blend. As a result, during the main injection combustion, the difference of OH emission between the baseline diesel and the butanol blend was reduced. Further, the OH emission detected at 280 nm was always higher for BU40 due to lower adiabatic flame temperature of the butanol blend.

Acknowledgements

The authors would like to express their appreciation to Mr. A. Mazzei for the technical support in preparing the equipment and during the experiments.

Nomenclature

ASOI After Start Of Injection
ATDC After Top Dead Center
BRIC Brazil, Russia, India and China
BSFC Brake Specific Fuel Consumption
BTDC Before Top Dead Center
BU00 pure commercial fuel
BU20 Commercial fuel blended with 20% of butanol (vol)
BU40 Commercial fuel blended with 40% of butanol (vol)
CAD Crank Angle Degree
CCD Charge-Coupled Device
ECW Engine Combustion Work
EGR Exhaust Gas Recirculation
FSN Filter Smoke Number
FSOI Fuel Delivery Start Of Injection
GHG Greenhouse Gases
MCC Mixing Controlled Combustion
PM Particulate Matter
SOI Start Of Injection
TDC Top Dead Center
UV Ultraviolet

References

1. Yan YJ, Li X, Wang GL, et al. (2014) Biotechnological preparation of biodiesel and its high-valued derivatives: A review. *Appl Energ* 113: 1614-1631.
2. Singh B, Guldhe A, Rawat I, et al. (2014) Towards a sustainable approach for development of biodiesel from plant and microalgae. *Renew Sust Energ Rev* 29: 216-245.
3. Swana J, Yang Y, Behnam M, et al. (2011) An analysis of net energy production and feedstock availability for biobutanol and bioethanol. *Bioresource Technol* 102 (2): 2112-2117.
4. Abdehagh N, Tezel FH, Thibault J (2014) Separation techniques in butanol production: Challenges and developments. *Biomass Bioenerg* 60: 222-246.
5. Yilmaz N (2012) Comparative analysis of biodiesel, ethanol, diesel and biodiesel methanol, diesel blends in a diesel engine. *Energy* 40(1): 210-213.
6. van der Merwe AB, Cheng H, Görgens JF (2013) Comparison of energy efficiency and economics of process designs for biobutanol production from sugarcane molasses. *Fuel* 105: 451-458.
7. Han SH, Cho DH, Kim YH, et al. (2013) Biobutanol production from 2-year-old willow biomass by acid hydrolysis and acetone-butanol-ethanol fermentation. *Energy* 61: 13-17.
8. García V, Päkkilä J, Ojamo H, et al. (2011) Challenges in biobutanol production: How to improve the efficiency? *Renew Sust Energ Rev* 15(2): 964-980.
9. Xue C, Zhao XQ, Liu CG, et al. (2013) Prospective and development of butanol as an advanced biofuel. *Biotechnol Adv* 31(8): 1575-1584.
10. Jin C, Yao MF, Liu HF, et al. (2011) Progress in the production and application of n-butanol as a biofuel. *Renew Sust Energ Rev* 15(8): 4080-4106.
11. Giakoumis EG, Rakopoulos CD, Dimaratos AM, et al. (2013) Exhaust emissions with ethanol or n-butanol diesel fuel blends during transient operation: A review. *Renew Sust Energ Rev* 17: 170-190.
12. Siwale L, Kristóf L, Adam T, et al. (2013) Combustion and emission characteristics of n-butanol/diesel fuel blend in a turbo-charged compression ignition engine. *Fuel* 107: 409-418.
13. Yao MF, Wang H, Zheng ZQ, et al. (2010) Experimental study of n-butanol additive and multi-injection on HD diesel engine performance and emissions. *Fuel* 89(9): 2191-2201.
14. Merola SS, Tornatore C, Iannuzzi SE, et al. (2014) Combustion process investigation in a high speed diesel engine fuelled with n-butanol diesel blend by conventional methods and optical diagnostics. *Renew Energ* 64: 225-237.
15. Valentino G, Corcione FE, Iannuzzi SE, et al. (2012) Experimental study on performance and emissions of a high speed diesel engine fuelled with n-butanol diesel blends under premixed low temperature combustion; *Fuel*, 92 (1): 295-307
16. Agarwal AK, Srivastava DK, Dhar A, et al. (2013) Effect of fuel injection timing and pressure on combustion, emissions and performance characteristics of a single cylinder diesel engine. *Fuel* 111: 374-383.
17. Chen Z, Liu J, Han Z, et al. (2013) Study on performance and emissions of a passenger-car diesel engine fueled with butanol–diesel blends. *Energy* 55: 638–646.
18. Zhao H, Ladommatos (2011) N Engine combustion instrumentation and diagnostics. *Soc Automot Eng*, Inc. USA.
19. Dec JE, Espey C (1988) Chemiluminescence Imaging of Autoignition in a DI Diesel Engine. SAE Technical Paper.

20. Zhao H, Ladommatos N (1998) Optical diagnostics for soot and temperature measurement in diesel engines. *Prog Energ Combust* 24(3): 221-255.
21. Kosaka H, Aizawa T, Kamimoto T (2005) Two-dimensional imaging of ignition and soot formation processes in a diesel flame. *J Eng Res* 6(1): 21-42,.
22. Heywood JB (1988) "Internal Combustion Engine Fundamentals", McGraw-Hill Inc.
23. Dieke GH, Crosswhite HM (1962) The ultraviolet bands of OH Fundamental data. *J Quant Spectrosc Radiat Trans* 2: 97-199.
24. Krishnamahari S, Broida H (1961) Effect of molecular oxygen on the emission spectra of atomic oxygen-acetylene flames. *J Chem Phys* 34: 1709-1711.
25. Tinaut FV, Reyes M, Giménez B, et al. (2011) Measurements of OH* and CH* Chemiluminescence in Premixed Flames in a Constant Volume Combustion Bomb under Autoignition Conditions. *Energ Fuels* 25(1): 119-129.
26. Gaydon AG, Wolfhard HG (1953) "Mechanism of formation of CH, C2, OH and HCO radicals in flames." Symposium (International) on Combustion 4(1): 211-218.
27. Fontijn A (1966) Mechanism of Chemiluminescence of AtomicOxygen—Hydrocarbon Reactions. Formation of the Vaidya Hydrocarbon Flame Band Emitter. *J Chem Phys* 44: 1702.
28. Gaydon AG (1957) The Spectroscopy of Flames. John Wiley & Sons, Inc., New York.
29. Tree DR, Svensson KI (2007) Soot processes in compression ignition engines. *Prog Energ Combust* 33(3): 272-309.
30. Senda J, Choi D, Iwamuro M, et al. (2002) Experimental Analysis on Soot Formation Process In DI Diesel Combustion Chamber by Use of Optical Diagnostics; SAE Technical Paper n.2002-01-0893.